2023

Deactivation Effects of Tb3+ on Ho3+ Emission in Fluoroindate Glasses for 3.9 μm Laser Applications

Zhi Zhang
Harbin Engineering University, China

Zhuowei Cheng
Harbin Engineering University, China

Ruicong Wang
Harbin Engineering University, China

See next page for additional authors

Funder: National Natural Science Foundation of China (Grant Nos. 61905048, 61935006, 62005060, 62005061, 62090062), Heilongjiang Provincial Natural Science Foundation of China (No. LH2020F030), National Key Research and Development Program of China (Grant No. 2020YFA0607602), Shenzhen Basic Research Foundation (Grant Nos. JCYJ20190808140805488, JCYJ20190808173619062), 111 Project (No. B13015) and Fundamental Research Funds for the Central Universities.

Deactivation effects of Tb^{3+} on Ho^{3+} emission in fluoroindate glasses for 3.9 μm laser applications

Zhi Zhang[1], Zhuowei Cheng[1], Ruicong Wang[1], Shunbin Wang[1], Gerald Farrell[2], Shijie Jia[1,*], Pengfei Wang[1,3,*]

[1]*Key Laboratory of In-fiber Integrated Optics, Ministry Education of China, Harbin Engineering University, Harbin 150001, China*

[2]*Photonics Research Center, Technological University Dublin, Grangegorman Campus, Dublin 7, Ireland*

[3]*Key Laboratory of Optoelectronic Devices and Systems of Ministry of Education and Guangdong Province, College of Optoelectronic Engineering, Shenzhen University, Shenzhen 518060, China*

Corresponding author: jiasj@hrbeu.edu.cn(S. Jia); pengfei.wang@tudublin.ie(P. Wang)

Keywords: *Fluoride glass; fluorescence; Mid-infrared; Rare-earth ion doping*

Abstract

A series of Ho^{3+}/Tb^{3+} co-doped fluoroindate glasses with good thermal stability have been synthesized to study the deactivation effects of Tb^{3+} on the Ho^{3+}: 3.9 μm emission. Efficient 3.9 μm emission enhancement is obtained under excitation by an 888 nm laser diode (LD). The Judd-Ofelt (J-O) intensity parameters and radiative properties are calculated to evaluate the spectroscopic properties. Possible energy transfer processes resulting in emission reinforcement are discussed. A higher spontaneous transition probability and larger peak emission cross section are achieved with the inclusion of Tb^{3+}. This analysis supports the conclusion that Ho^{3+}/Tb^{3+} co-doped fluoroindate glass is a potentially useful laser material for highly efficient 3.9 μm fiber lasers.

1. Introduction

As the 3-5 μm region overlaps with several common characteristic absorption wavelengths of gas molecules and possesses extremely high atmospheric transmittance, lasers operating in the 3-5 μm region are of great interest in an increasing number of applications including gas monitoring, remote sensing, medical treatment and advanced radars [1-5]. To satisfy the need of laser sources for these applications, rare-earth (RE) doped fiber lasers have been considered as attractive candidates [6, 7], as they offer potential advantages including improved beam quality, robustness and high average output power [8]. The maximum average output power reported to date for fiber lasers operating at 3 μm and 3.5 μm are 70 W and 15 W, respectively [9, 10]. Compared to fiber lasers operating in the region 3-3.5 μm, there has been little research carried out on 3.9 μm fiber laser emission generated by the transition of Ho^{3+}: $^5I_5 \rightarrow {}^5I_6$, although fluoride fiber lasers have provided the longest wavelength [11, 12]. In 1997, by employing a pump wavelength at 890 nm and improved resonator cavity, lasing at 3.9 μm was achieved and an improved average output power of 11 mW was demonstrated [13, 14]. However, it still required a cooling environment as the multi-phonon decay of Ho^{3+} ions in ZBLAN(ZrF_4-BaF_2-LaF_3-AlF_3-NaF) fiber generated a significant excess heat. The principal reasons for low output power in ZBLAN fibers are the high intrinsic phonon energy of ZBLAN glass and the self-termination effect of the Ho^{3+}: $^5I_5 \rightarrow {}^5I_6$ transition [15]. To solve the first problem, fluoroindate glass has been considered, as it provides a lower phonon energy and a broader transmission window compared to

ZBLAN glass [16]. This glass has been successfully drawn into low-loss fibers and is useful for broadband supercontinuum generation and mid-infrared fiber lasing [17-20].

The self-termination effect of the Ho^{3+}: $^5I_5 \rightarrow {}^5I_6$ transition, in similar manner to the transition of Er^{3+}: $^4I_{9/2} \rightarrow {}^4I_{11/2}$ [21], results from the fact that the lifetime of the upper state $^5I_5$ is much shorter than that of the lower state $^5I_6$ [22]. In 2018, an output power of 200 mW with a slope efficiency of 10.2% at room temperature was obtained at 3.92 μm in a cladding-pumped Ho^{3+}-doped fluoroindate fiber laser [23]. To suppress the self-termination effect, heavily Ho^{3+}-doped fluoroindate fiber was used to deplete the $^5I_6$ state through the energy transfer up-conversion (ETU) process ($^5I_6 + {}^5I_6 \rightarrow {}^5F_5 + {}^5I_8$).

In addition to the above approaches, energy transfer processes between RE ions have been investigated to deactivate the undesired long-lifetime of a lower laser state. In 2019, Li et al. demonstrated that the energy transfer from Er^{3+}: $^4I_{13/2}$ to Eu^{3+}: $^7F_6$ enhanced the 2.75 μm emission in Er^{3+}/Eu^{3+} doped PbF_2 crystals [24]. In 2020, the sensitization and deactivation effects of Nd^{3+} on the lower state of Ho^{3+}: $^5I_6$ were investigated in fluoroindate glasses [25]. Yet, appropriate RE ions that can improve the luminescence efficiency of the Ho^{3+}: $^5I_5 \rightarrow {}^5I_6$ transition are still under investigation.

In this work, we report the investigation of the luminescence properties and energy transfer mechanisms of Ho^{3+}-doped and Ho^{3+}/Tb^{3+}-co-doped fluoroindate glasses to identify the effects on the 3.9 μm emission of this co-doping system. The emission spectra and fluorescence decay properties have been measured, and Judd-Ofelt parameters have been calculated. The above optical properties have been assessed to

demonstrate the feasibility of Ho^{3+}/Tb^{3+}-codoped fluoroindate glasses for future applications in 3.9 μm fiber-lasers.

2. Experiment

The molar compositions of glass samples used in this investigation were $(30.5-x)InF_3$-$20ZnF_2$-$20SrF_2$-$16BaF_2$-$6GaF_3$-$6CaF_2$-$1.5HoF_3$-$xTbF_3$, where x=0, 0.1, 0.2, 0.3, 0.4, 0.5. These glasses were named as 1.5Ho-xTb. By employing a traditional melt quenching procedure [26], all chemicals were mixed from high purity (99.99%) raw materials. To avoid excessive water in the glass, all processes were carried out in a glove box filled with dry nitrogen. The prepared materials were completely melted in a Pt-Au crucible at 900 ℃ for 2 h, then annealed at 280 ℃ for a further 3 h, and finally naturally cooled down to room temperature to remove internal stress. The glasses were then polished for subsequent tests.

The experimental absorption spectra were measured by a Perkin-Elemer Lambda 750 UV-VIS-NIR spectrophotometer, while transmission spectra were measured using a Perkin-Elmer FTIR spectrometer. The infrared fluorescence spectra were tested using an Edinburg FLS1000 spectrometer. Differential scanning calorimetry (DSC) was analyzed using a NETZSCH DSC 204 F1 calorimeter. In the fluorescence lifetime test, the glass samples were excited employing a modulated Surelite OPO pulsed laser. Each measurement was performed at room temperature.

3. Result and Discussion

3.1 Vibrational characteristic and thermal stability

The Raman spectra of fluoroindate glass with gaussian fit was shown in Figure 1. The bands centered at 207 cm^{-1} is probably the bending modes of Ho-F and Tb-F together with asymmetric Zn-F and Ba-F stretching vibrations [27], previously reported in fluorozirconate glasses [28]. The band at 421 cm^{-1} and 507 cm^{-1} are in relation to symmetric stretching vibrations of bridge fluorine atoms of In-F_b-In and non-bridged (nb) fluorine atoms F_{nb}-In-F_{nb} in octahedrons [InF_6] [29]. The 618 cm^{-1} band is on account of symmetrical stretching vibrations of non-bridged fluorine atoms in [GaF_4] tetrahedrons [30, 31].

The DSC curve of the glass sample was measured for characteristic temperatures, including the glass transition temperature T_g and the crystallization temperature T_x, as shown in inset of Fig. 2(a). The evaluated $\Delta T(T_x - T_g)$ of the fluoroindate glass in our work is 79.1 °C, indicating that this particular composition has good thermal stability against crystallization during the fiber-fabrication process [32] and thus is a promising glass material for low-loss fibers [33].

3.2 Absorption spectra, and Judd-Ofelt analysis

The refractive index and density values for the fluoroindate glass are 1.493 and 5.134 g/cm^3, respectively. Figure 2(b) shows the absorption spectra of the samples in the wavelength range of 400-2400 nm at room temperature. The strong absorption band of Ho^{3+}: $^5I_5$ in the wavelength range 880-920 nm suggests that the Ho^{3+} ions of glasses can be directly excited by an 888 nm LD. The transmission spectra of fluoroindate glass

within the 1500-12000 nm wavelength range is shown in the inset of Fig. 2(a). It is worth noting that the glass samples exhibit excellent transmittance (more than 90%) over the wavelength range 1500-7000 nm, with an infrared cutoff wavelength of approximately 12000 nm. Furthermore, the calculated absorption associated to OH (α_{OH-}) is as little as 0.23 ppm in a bulk glass 1 cm long [34], indicating that the undesirable energy transfer from Ho^{3+} to OH^- is very weak and consequently has little effect on the mid-IR emission [35].

The spectroscopic parameters Ω_2, Ω_4, Ω_6 of Ho^{3+} in the glasses are calculated using the Judd-Ofelt theory [36, 37] and the measured absorption spectra. Table 1 shows a comparison of spectroscopic parameters in various glasses. As expected, the Ω_2 in the Ho^{3+}/Tb^{3+} co-doped sample is higher than that in Ho^{3+} single doped sample, indicating that a lower symmetry and higher covalency for surrounding Ho^{3+} ions are generated by the introduction of Tb^{3+} ions [38, 39]. In contrast, the parameters Ω_4 and Ω_6 are associated with the viscosity and rigidity of the glass host [40]. The grown spectroscopic quality factor Ω_4/Ω_6 in this case denotes that additive deactivated Tb^{3+} ions favor the energy transfer process Ho^{3+}: $^5I_5 \rightarrow {}^5I_6$ [41].

Table 2 lists the calculated radiative parameters of the various transitions among corresponding energy levels of Ho^{3+} ions in the foundation of the acquired J-O intensity parameters [42]. The value of A of the Ho^{3+}: $^5I_5 \rightarrow {}^5I_6$ transition in the Ho^{3+}/Tb^{3+} co-doped fluoroindate glass is calculated to be 5.70 s^{-1}, which is larger than that in the Ho^{3+} single doped fluoroindate glass (5.02 s^{-1}) and in the ZBYA glass (2.96 s^{-1}) [43],

suggesting that the introduction of Tb^{3+} ions is advantageous to the Ho^{3+}: 3.9 μm fluorescence emission efficiency in fluoroindate glass.

3.3 Infrared fluorescence properties and energy transfer mechanism

Figure 3 and 4 show the MIR and NIR fluorescence spectra of Ho^{3+} doped and Ho^{3+}/Tb^{3+} co-doped glasses, resulting from the $^5I_5 \rightarrow {}^5I_6$, $^5I_6 \rightarrow {}^5I_7$, $^5I_7 \rightarrow {}^5I_8$, $^5I_5 \rightarrow {}^5I_7$, $^5I_6 \rightarrow {}^5I_8$ transitions of Ho^{3+}. Under the excitation of an 888 nm LD, the emission intensity at 3.9 μm is increased by ~30% after the inclusion of Tb^{3+}, indicating that $^5I_6$ level has been depopulated by the introduced Tb^{3+}, resulting in an enhanced 3.9 μm emission. The emission spectra have a full width at half maximum (FWHM) of 97 nm, which is similar to that of ZBYA glass [43]. It is worth mentioning that concentration quenching of the 3.9 μm emission does not appear until the Tb^{3+} concentration reaches 0.3 mol.%. Concentration quenching may be caused by the increased proximity of Ho^{3+} and Tb^{3+} ions resulting from the increased concentration of Tb^{3+}. Fig. 4(c) shows that a similar effect has been observed also in the 1.7 μm emission, indicating the deactivation effects of Tb^{3+} acts on the energy transfer of $^5I_5 \rightarrow {}^5I_7$. Furthermore, Fig. 4 shows that other emissions with peak wavelengths located at 1.2 μm, 2.0 μm and 2.9 μm exhibit a uniform declining tendency due to the depopulation of $^5I_6$ and $^5I_7$ states caused by the possible energy transfer between Ho^{3+} and Tb^{3+} ions.

Based on the above results, a possible energy transfer mechanism schematic for the Ho^{3+}/Tb^{3+} system under the excitation of an 888 nm LD is described in Fig. 5. Firstly, Ho^{3+} ions are excited to the upper state $^5I_5$ from $^5I_8$ by ground state absorption (GSA). After the

introduction of Tb^{3+} ions, a portion of the Ho^{3+} ions on the $^5I_6$ state transfer energy to the adjacent Tb^{3+}: $^7F_0$ level via the ET1 process. Similarly, energy transmission takes place on account of the ET2 process between Ho^{3+}: $^5I_7$ and Tb^{3+}: $^7F_2$. Furthermore, the cross-relaxation (CR1) process: Ho^{3+}: $^5I_6$ + Tb^{3+}: $^7F_6 \rightarrow Ho^{3+}$: $^5I_7$ + Tb^{3+}: $^7F_4$ also quenches the lower state $^5I_6$ to enhance the 3.9 μm emission. The above processes work together to reduce the population of $^5I_6$, and thus enhance population inversion for the Ho^{3+}: $^5I_5 \rightarrow {}^5I_6$ transition.

3.4 Fluorescence decay curves and calculated cross section

To further investigate the energy interaction mechanism between donor Ho^{3+} and acceptor Tb^{3+} ions, the fluorescence decay curves of the Ho^{3+}: $^5I_5$ and Ho^{3+}: $^5I_6$ energy levels of Ho^{3+}/Tb^{3+} co-doped and Ho^{3+} singly doped samples were measured under the excitation of an 888 nm pulsed laser, as shown in Fig. 6. The lifetime of the $^5I_5$ level does not show any significant change after the inclusion of Tb^{3+}. On the contrary, the lifetime of both lower levels $^5I_6$ and $^5I_7$ exhibit a gradually decreasing tendency as the Tb^{3+} concentration increases. According to the ET processes described above, the lifetime of the $^5I_6$ level in the Ho^{3+}/Tb^{3+} co-doped glasses (0.66 ms) is much shorter than that in the Ho^{3+} singly doped glass (3.86 ms). The quantum efficiency of ET between Ho^{3+} and Tb^{3+} was calculated using the following equation [39]: $\eta=1-\tau_{Ho/Tb}/\tau_{Ho}$, where τ_{Ho} and $\tau_{Ho/Tb}$ are the lifetimes of $^5I_6$ state of Ho^{3+}-doped and Ho^{3+}/Tb^{3+} co-doped fluoroindate glasses, respectively. The quantum efficiency of ET is calculated to be 61.6% and the results confirm that Tb^{3+} can be used as an effective deactivation ion to depopulate Ho^{3+}: $^5I_6$ and enhance emission at 3.9 μm.

In order to assess the gain properties for emission at 3.9 μm, the emission cross-sections were calculated using the following Fuchtbauer-Ladenburg equation [44]:

$$\sigma_{emi} = \frac{\lambda^4 A_{\text{rad}}}{8\pi c n^2} \times \frac{\lambda I(\lambda)}{\int \lambda I(\lambda) d\lambda} \tag{1}$$

where λ is the wavelength. A_{rad} is the spontaneous transition probability and $I(\lambda)$ is the measured fluorescence intensity at wavelength λ. Additionally, n and c are the refractive index and speed of light in a vacuum, respectively.

The absorption cross-sectional area σ_{abs} can be derived from by σ_{emi} using McCumber theory [45]:

$$\sigma_{abs} = \sigma_{emi} \times \left(\frac{Z_u}{Z_l} \right) \times \left[\frac{-\left(E_{zl} - \hbar c \lambda^{-1} \right)}{kT} \right] \tag{2}$$

In this formula, $\hbar$ is Planck's constant, k is Boltzmann's constant, T is the temperature, E_{zl} is the energy gap between the ground state level and the excitation level and Z_u, Z_l denote the partition functions of the upper and lower states, respectively. The maximum emission cross section in the Ho^{3+}/Tb^{3+} co-doped glass was calculated to be 6.53×10^{-21} cm^2 at 3930 nm, significantly higher than that (5.71×10^{-21} cm^2) in the Ho^{3+} doped glass, as shown in Fig. 7. This suggests that the participation of Tb^{3+} ions will significantly increase the possibility of lasing at 3.9 μm.

3.5 Population densities

To investigate the effect of co-doping with Tb^{3+} on population densities, a series of rate equations for 888 nm pumping were established, based on the model shown in Fig.

5. The small contribution of up-conversion is neglected to simplify the rate equations. The rate equations thus are given by

$$\frac{dn_4}{dt} = \sigma_{14}\phi n_1 - \left(\frac{1}{\tau_4} + W_{mpr4} + C_{45}n_5\right)n_4 \tag{3}$$

$$\frac{dn_3}{dt} = -\left(\frac{1}{\tau_3} + W_{mpr3} + C_{35}n_5 + W_{ET1}n_5\right)n_3 + \left(\frac{1}{\tau_4}\beta_{43} + W_{mpr4} + C_{45}n_5\right)n_4 \tag{4}$$

$$\frac{dn_2}{dt} = -\left(\frac{1}{\tau_2} + W_{ET2}n_5\right)n_2 + \left(\frac{1}{\tau_3}\beta_{32} + W_{mpr3} + C_{35}n_5\right)n_3 + \frac{1}{\tau_4}\beta_{42}n_4 \tag{5}$$

$$\frac{dn_1}{dt} = -\sigma_{14}\phi n_1 + \frac{1}{\tau_2}n_2 + \frac{1}{\tau_3}\beta_{31}n_3 + \frac{1}{\tau_4}\beta_{41}n_4 \tag{6}$$

where n_i is the population of the i level as illustrated in Fig. 4 ($n_1+n_2+n_3+n_4+n_5 = 3.12\times10^{20}$ cm^{-3}). σ_{14} is the ground state absorption cross section (from Ho^{3+}: $^5I_8$ to Ho^{3+}: $^5I_5$). W_{mpri} and τ_i are the multi-phonon relaxation rate and the radiative lifetime of the i level, respectively. C_{35} and C_{45} are the cross relaxation coefficients of CR1 and CR2 (Ho^{3+}: $^5I_5$ + Tb^{3+}: $^7F_6 \rightarrow Ho^{3+}$: $^5I_6$ + Tb^{3+}: $^7F_5$), respectively. W_{ET1} and W_{ET2} are the energy transfer rates of ET1 and ET2. β_{ij} is the calculated branching ratio of the energy transition from i level to j level. The pump flux ϕ is obtained from:

$$\phi = \frac{H\lambda}{\hbar c} \tag{7}$$

where H is the pump power density (1.59×10^5 W/m^2) and λ is the pump light wavelength (888 nm). $\hbar$ and c are the Planck constant and light speed in a vacuum, respectively.

Based on the above equations, the steady-state population of the $^5I_5$ level was performed using [46]:

$$n_4 = \frac{\sigma_{14}\phi n_1}{\frac{1}{\tau_4} + W_{mpr4} + C_{45}n_5} \tag{8}$$

To simplify the calculation process, the populations of the ground state of Ho^{3+} (n_1) and Tb^{3+} (n_5) are assumed to be equal to the doping concentration of Ho^{3+} and Tb^{3+}, respectively. W_{mpr4} and C_{45} can be calculated from:

$$\frac{1}{\tau_{m4}} = \frac{1}{\tau_{r4}} + W_{mpr4} + C_{45}n_5 \tag{9}$$

where τ_{m4} and τ_{r4} are the measured and calculated radiative lifetime of the $^5I_5$ level, respectively. Therefore, the dependence of n_4 on concentrations can be calculated. The populations of the $^5I_6$ level (n_3) is obtained by [47]:

$$\frac{n_4}{n_3} = \left(\frac{A_3}{\beta_{43}A_4}\right)\frac{\int \lambda I_{3.9\mu m}(\lambda)d\lambda}{\int \lambda I_{1.2\mu m}(\lambda)d\lambda} \tag{10}$$

where A_3 and A_4 are the calculated radiative transition probabilities of the $^5I_6$ and $^5I_5$ levels, respectively. Figure 8 shows the population densities of the two levels for different Tb^{3+} concentrations calculated from the equations above. For increasing Tb^{3+} concentration, the calculated population of $^5I_5$ rises slightly due to the larger absorption cross section of $^5I_8 \rightarrow {}^5I_5$, while that of the lower level $^5I_6$ drops substantially because of the ET processes proposed.

4. Conclusion

In conclusion, Ho^{3+} doped and Ho^{3+}/Tb^{3+} co-doped fluoroindate glasses have been fabricated. The introduction of Tb^{3+} resulted in a high spontaneous transition probability and large emission cross section. Compared to the Ho^{3+} doped sample, enhanced 3.9 μm

emission was obtained under excitation by an 888 nm LD. An energy transfer mechanism explained how Tb^{3+} exerted a positive effect on the population inversion of the $^5I_5 \rightarrow {}^5I_6$ transition. These achievements show that Ho^{3+}/Tb^{3+} co-doped fluoroindate glasses could be promising materials for a 3.9 μm fiber lasers.

Acknowledgment

This work was financially supported by the National Natural Science Foundation of China (Grant Nos. 61905048, 61935006, 62005060, 62005061, 62090062), Heilongjiang Provincial Natural Science Foundation of China (No. LH2020F030), National Key Research and Development Program of China (Grant No. 2020YFA0607602), Shenzhen Basic Research Foundation (Grant Nos. JCYJ20190808140805488, JCYJ20190808173619062), 111 Project (No. B13015) and Fundamental Research Funds for the Central Universities (Grant Nos. 3072021CF2514, 3072021CF2533).

References

[1] W. Wang, B. Zhou, S. Xu, Z. Yang, Q. Zhang, Recent advances in soft optical glass fiber and fiber lasers, Prog. Mater. Sci., 101 (2019) 90-171.

[2] M. R. Majewski, R. I. Woodward, S. D. Jackson, Dysprosium mid-infrared lasers: Current status and future prospects, Laser Photonics Rev., 14 (2020) 1900195.

[3] Z. Wang, B. Zhang, J. Liu, Y. Song, H. Zhang, Recent developments in mid-infrared fiber lasers: Status and challenges, Opt. Laser Technol., 132 (2020) 106497.

[4] M. C. Falconi, D. Laneve, F. Prudenzano, Advances in Mid-IR fiber lasers: tellurite, fluoride and chalcogenide, Fibers, 5 (2017) 23.

[5] S. D. Jackson, Towards high-power mid-infrared emission from a fibre laser, Nat. Photonics, 6 (2012) 423-431.

[6] C. Liu, S. Feng, X. Xiao, Y. Xu, H. Guo, Intense 2.85 μm mid-infrared emissions in Yb^{3+}/Ho^{3+} codoped and $Yb^{3+}/Er^{3+}/Ho^{3+}$ tridoped TBLL fluorotellurite glasses and their energy transfer mechanism, Ceram. Int., 48 (2022) 5267-5273.

[7] C. Zhang, S. Zhao, D. Deng, L. Huang, Y. Tian, S. Xu, Influence of LaF_3 on the crystallization and luminescence of Eu^{3+}-doped oxyfluoride glass ceramics, Ceram. Int., 40 (2014) 2737-2740.

[8] C. Yuan, Y. Jiang, L. Zhang, Z. Wang, Y. Guo, Y. Jiang, S. Cui, Y. Li, L. Wang, J. Li, M. Liao, H. Zeng, L. Zhang, Glass-forming ability control of Er^{3+}-Doped lithium-modified fluorozirconate glass, Ceram. Int., 45 (2019) 24115-24120.

[9] G. A. Newburgh, M. Dubinskii, Power and efficiency scaling of Er: ZBLAN fiber laser, Laser Phys. Lett., 18 (2021) 095102.

[10] M. Lemieux-Tanguay, V. Fortin, T. Boilard, P. Paradis, F. Maes, L. Talbot, R. Vallée, M. Bernier, 15 W monolithic fiber laser at 3.55 μm, Opt. Lett., 47 (2022) 289-292.

[11] J. J. Nunes, L. Sojka, R. W. Crane, D. Furniss, Z. Tang, D. Mabwa, B. Xiao, T. M. Benson, M. Farries, N. Kalfagiannis, E. Barney, S. Phang, A. B. Seddon, S. Sujecki, Room temperature mid-infrared fiber lasing beyond 5 μm in chalcogenide glass small-core step index fiber, Opt. lett., 46 (2021) 3504-3507.

[12] C. Zhang, C. Zhang, C. Yun, S. Lai, Intense broadband 3.1 μm emission in Er^{3+}-doped fluoroaluminate-tellurite glass for mid-infrared laser application, Ceram. Int., 48 (2022) 29977-29981

[13] J. Schneider, Fluoride fibre laser operating at 3.9 μm, Electron. Lett., 31 (1995) 1250-1251.

[14] J. Schneider, C. Carbonnier, U. B. Unrau, Characterization of a Ho^{3+}-doped fluoride fiber laser with a 3.9 μm emission wavelength, Appl. Opt., 36 (1997) 8595-8600.

[15] L. Gomes, V. Fortin, M. Bernier, R. Vallée, S. Poulain, M. Poulain, S. D. Jackson, The basic spectroscopic parameters of Ho^{3+}-doped fluoroindate glass for emission at 3.9 μm, Opt. Mater., 60 (2016) 618-626.

[16] M. Kochanowicz, M. Lesniak, J. Zmojda, P. Miluski, A. Baranowska, T. Ragin, M. Kuwik, W.A. Pisarski, J. Pisarska, J. Dorosz, D. Dorosz, Structure, luminescence and energy transfer of fluoroindate glasses co-doped with Er^{3+}/Ho^{3+}, Ceram. Int., 46 (2020) 26403-26409.

[17] J. Bei, T. M. Monro, A. Hemming, H. Ebendorff-Heidepriem, Fabrication of extruded fluoroindate optical fibers, Opt. Mater. Express, 3 (2013) 318-328.

[18] L. Yang, B. Zhang, X. He, K. Deng, S. Liu, and J. Hou, High-power mid-infrared supercontinuum generation in a fluoroindate fiber with over 2 W power beyond 3.8 μm, Opt. Express, 28 (2020) 14973-14979.

[19] S. Jia, Z. Jia, C. Yao, L. Zhang ,Y. Feng, G. Qin, Y. Ohishi, W. Qin, 2875 nm lasing from Ho^{3+}-doped fluoroindate glass fibers, IEEE Photon. Technol. Lett., 30 (2018)

323-326.

[20] H. He, Z. Jia, T. Wang, Y. Ohishi, W. Qin, G. Qin, Intense emission at ~3.3 μm from Er^{3+}-doped fluoroindate glass fiber, Opt. lett., 46 (2021) 1057-1060.

[21] F. Huang, L. Hu, D. Chen, NIR to visible upconversion in Er^{3+}-doped fluoride glass under 1550 and 980 nm excitations, Ceram. Int., 41 (2015) 189-193.

[22] L. Gomes, V. Fortin, M. Bernier, F. Maes, R. Vallée, S. Poulain, M. Poulain, S. D. Jackson, Excited state absorption and energy transfer in Ho^{3+}-doped indium fluoride glass, Opt. Mater., 66 (2017) 519-526.

[23] F. Maes, V. Fortin, S. Poulain, M. Poulain, J.-Y. Carrée, M. Bernier, R. Vallée, Room-temperature fiber laser at 3.92 μm, Optica, 5 (2018) 761-764.

[24] X. Li, P. Zhang, S. Zhu, H. Yin, Z. Li, Z. Chen, Y. Zheng, J. Yu, Enhanced 2.75 μm emissions of Er^{3+} via Eu^{3+} deactivation in PbF_2 crystal, J. Lumines., 210 (2019) 164-168.

[25] R. Wang, J. Zhang, H. Zhao, X. Wang, S. Jia, H. Guo, S. Dai, P. Zhang, G. Brambilla, S. Wang, P. Wang, 3.9 μm emission and energy transfer in ultra-low OH^-, Ho^{3+} /Nd^{3+} co-doped fluoroindate glasses, J. Lumines., 225 (2020) 117363 (2020).

[26] J. Xing, F. Shang, L. Li, G. Chen, Structure, up-conversion luminescence and optical temperature sensitive properties of glass ceramics containing $Ca_5(PO_4)_3F$ with double luminescence centers, Ceram. Int., 48 (2022) 1098-1106.

[27] B. Bendow, P. K. Banerjee, M. G. Drexhage, J. Goltman, S. S. Mitra, C. T. Moynihan, Comparative Study of Vibrational Characteristics of Fluorozirconate

and Fluorohafnate Glasses, J. Am. Ceram. Soc., 65 (1982) C-8-C-9.

[28] B. Bendow, P. K. Banerjee, J. Lucas, G. Fonteneau, M. G. Drexhage, Polarized Raman Scattering in Rare-Earth Fluoride Glasses, J. Am. Ceram. Soc., 68 (1985) C-92-C-95.

[29] R. M. Almeida, J. C, Pereira, Y. Messaddeq, M. A. Aegerter, Vibrational spectra and structure of fluoroindate glasses, J. Non-Cryst. Solids, 161 (1993) 105-108.

[30] L. Zhou, F. Huang, B. Dou, Y. Li, R. Ye, H. Wang, S. Xu, Sensitization effect between Ln^{3+} ions in zinc fluoride glasses for MIR applications, Ceram. Int., 45 (2019) 10640-10645.

[31] R. Szal, J. Zmojda, M. Kochanowicz, P. Miluski, J. Dorosz, M. Lesniak, P. Jeleń, B. Starzyk, M. Sitarz, M. Kuwik, J. Pisarska, W.A. Pisarski, Y. Iijima, T. Mori, D. Dorosz, Spectroscopic properties of antimony modified germanate glass doped with Eu^{3+} ions, Ceram. Int., 45 (2019) 24811-24817.

[32] L. Xiao, W. Wang, H. Gao, Z. Hu, Y. Mao, Synthesis and optical properties of Bi^{3+}/Yb^{3+} co-doped transparent oxyfluoride glass-ceramics, Ceram. Int., 41 (2015) 10137-10141.

[33] S. Wang, J. Zhang, N. Xu, S. Jia, G. Brambilla, and P. Wang, 2.9 μm lasing from a Ho^{3+}/Pr^{3+} co-doped AlF_3-based glass fiber pumped by a 1150 nm laser, Opt. lett., 45 (2020) 1216-1219.

[34] E. Kolobkova, A. Alkhlef, L. Y. Mironov, O. Bogdanov, Effect of the phosphate content on the spectroscopic and lasing properties of Er^{3+}/Yb^{3+}-doped

fluorophosphate glasses, Ceram. Int., 46 (2020) 26396-26402.

[35] Z. Zhao, S. Jia, H. He, Z. Jia, W. Qin, and G. Qin, Study on 2.86 μm emission properties of Ho^{3+}-doped low-hydroxyl ZnF_2 based fluoride glasses for mid-infrared laser applications, Opt. Mater. Express, 10 (2020) 3137-3144.

[36] B. R. Judd, Optical absorption intensities of rare-earth ions, Phys. Rev., 127 (1962) 750-761.

[37] G. S. Ofelt, Intensities of crystal spectra of rare-earth ions, J. Chem. Phys., 37 (3) (1962) 511-520.

[38] F. Huang, Y. Tian, D. Chen, S. Xu, J. Zhang, Spectroscopic properties and energy transfer mechanism in Dy^{3+}/Tm^{3+} codoped fluoroaluminate glasses modified by TeO_2, Ceram. Int., 42 (2016) 132-137.

[39] L. Zhou, F. Huang, B. Dou, Y. Li, R. Ye, H. Wang, S. Xu, Sensitization effect between Ln^{3+} ions in zinc fluoride glasses for MIR applications, Ceram. Int., 45 (2019) 10640-10645.

[40] F. Huang, Y. Tian, S. Xu, J. Zhang, Spectroscopic and energy transfer mechanism of Er^{3+}, Pr^{3+}-codoped ZBYA glass, Ceram. Int., 42 (2016) 7924-7928.

[41] R. Cao, M. Cai, Y. Lu, Y. Tian, F. Huang, S. Xu, J. Zhang, Ho^{3+}/Yb^{3+} codoped silicate glasses for 2 μm emission performances, Appl. Opt., 55 (2016) 2065-2070.

[42] M. Liu, J. Zhang, J. Zhang, Z. Zhang, G. Farrell, G. Brambilla, S. Wang, P. Wang, 2.4 μm fluorescence of holmium doped fluoroaluminate glasses, J. Lumines., 238 (2021) 118265.

[43] H. Zhao, R. Wang, X. Wang, S. Jia, Y. Fan, E. Lewis, G. Farrell, S. Wang, P. Wang, Intense mid-infrared emission at 3.9 μm in Ho^{3+}-doped ZBYA glasses for potential use as a fiber laser, Opt. lett., 45 (2020) 4272-4275.

[44] S. A. Payne, L. L. Chase, L. K. Smith, W. L. Kway, W. F. Krupke, Infrared cross-section measurements for crystals doped with Er^{3+}, Tm^{3+}, and Ho^{3+}, IEEE J. Quantum Electron., 28 (1992) 2619-2330.

[45] D. E. McCumber, Einstein relations connecting broadband emission and absorption spectra, Phys. Rev., 136 (1964) A954-A957.

[46] T. H. Lee, J. Heo, Y. G. Choi, B. J. Park, W. J. Chung, Emission properties of Ho^{3+}/Tb^{3+} Co-doped in $Ge_{30}Ga_2As_8S_{60}$ glass, J. Appl. Phys., 96 (2004) 4827-4832.

[47] J. Ganem, J. Crawford, P Schmidt, N. W. Jenkins, S. R. Bowman, Thulium cross-relaxation in a low phonon energy crystalline host, Phys. Rev. B, 66 (2002) 245101.

Figure Captures

Fig. 1. Gaussian fit peaks of Raman spectrum in the fluoroindate glass.

Fig. 2. (a)Transmission spectrum of 1.5 mol.% Ho^{3+}-doped glass; (b)absorption spectra of 1.5 mol.% Ho^{3+}, 3mol.% Tb^{3+} singly doped and Ho^{3+}/ Tb^{3+} codoped glasses. Inset: differential scanning calorimetry curve in the temperature range 200-500 °C and photograph of glass samples.

Fig. 3. Emission spectra of Ho^{3+} single-doped and Ho^{3+}/Tb^{3+} co-doped glasses in the wavelength region 3650-4200 nm. Inset: dependence of the luminescence intensity on the concentration of Tb^{3+} ions.

Fig. 4. Fluorescence spectra of Ho^{3+} single-doped and Ho^{3+}/Tb^{3+} co-doped fluoroindate glasses in the wavelength region (a)2600-3200 nm; (b)1800-2200 nm; (c) 1550-1800 nm; and (d)1100-1280 nm.

Fig. 5. Energy level diagram and energy transfer process between Ho^{3+} and Tb^{3+} under 888 nm LD excitation**.**

Fig. 6. Luminescence decay curves of (a) the $^5I_5$ and (b) the $^5I_6$ energy levels; (c) experimental lifetimes of $^5I_5$ and $^5I_6$ levels; (d) measured lifetime of the $^5I_7$ level and the dependence of the $^5I_5$ to $^5I_6$ lifetime ratio for different Tb^{3+} concentrations.

Fig. 7. Absorption and emission cross-sections corresponding to $^5I_5 \rightarrow {}^5I_6$ transitions of Ho^{3+} in single-doped (solid line) and Ho^{3+}/Tb^{3+} co-doped (dash line) fluoroindate glasses.

Fig. 8. Population densities of $^5I_5$ and $^5I_6$ levels in glasses with different Tb^{3+} concentration.

Table 1. J-O parameters of Ho^{3+} in various glasses.

Glass Sample	Ω_2	Ω_4	Ω_6	Reference
1.5Ho	1.06	2.13	1.99	This work
1.5Ho-0.3Tb	1.10	2.50	2.24	
ZBYA	3.89	2.52	0.54	[43]

Table 2. Calculated Spontaneous Transition Probability(A), Branching Ratios (β) and Radiative Life Times (τ_{rad}) for various selected excited states of Ho^{3+} in singly doped and codoped samples.

Glass Sample	Transition	λ (nm)	A (s^{-1})	β (%)	τ_{rad} (ms)
1.5Ho	$^5I_5 \rightarrow {}^5I_6$	3920	5.02	3.65	7.26
	$\rightarrow {}^5I_7$	1680	74.96	54.47	
	$\rightarrow {}^5I_8$	889	57.64	41.88	
	$^5I_6 \rightarrow {}^5I_7$	2870	15.17	9.54	6.29
	$\rightarrow {}^5I_8$	1190	143.89	90.46	
	$^5I_7 \rightarrow {}^5I_8$	2020	58.05	100	17.23
1.5Ho-0.3Tb	$^5I_5 \rightarrow {}^5I_6$	3920	5.70	3.67	6.44
	$\rightarrow {}^5I_7$	1680	84.46	54.38	
	$\rightarrow {}^5I_8$	889	65.16	41.95	
	$^5I_6 \rightarrow {}^5I_7$	2870	17.15	9.56	5.57
	$\rightarrow {}^5I_8$	1190	162.26	90.44	
	$^5I_7 \rightarrow {}^5I_8$	2020	65.54	100	15.26

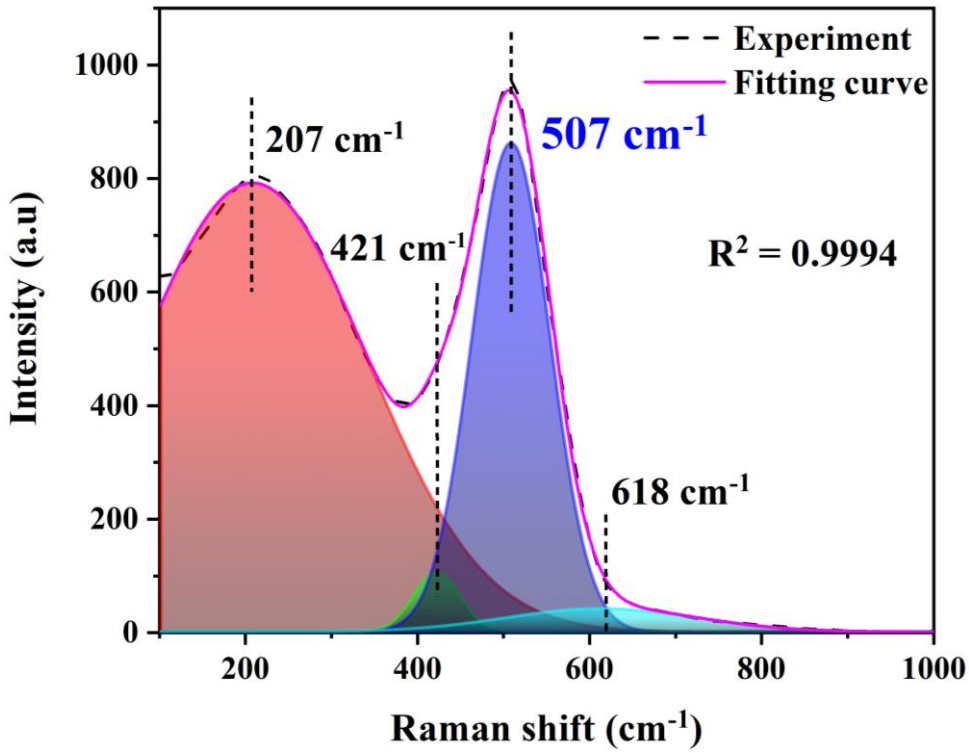

Fig. 1. Gaussian fit peaks of Raman spectrum in the fluoroindate glass.

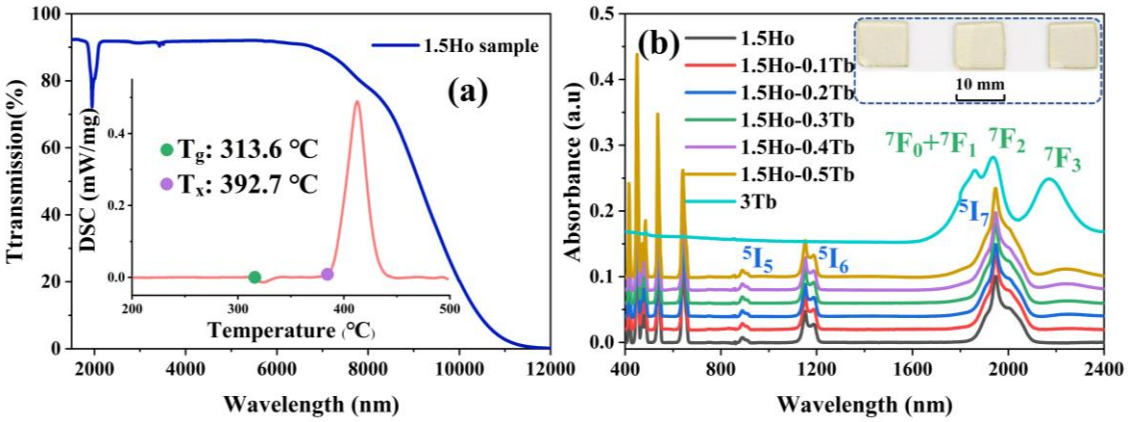

Fig. 2. (a)Transmission spectrum of 1.5 mol.% Ho^{3+}-doped glass; (b)absorption spectra of 1.5 mol.% Ho^{3+}, 3mol.% Tb^{3+} singly doped and Ho^{3+}/ Tb^{3+} codoped glasses. Inset: differential scanning calorimetry curve in the temperature range 200-500 ℃ and photograph of glass samples.

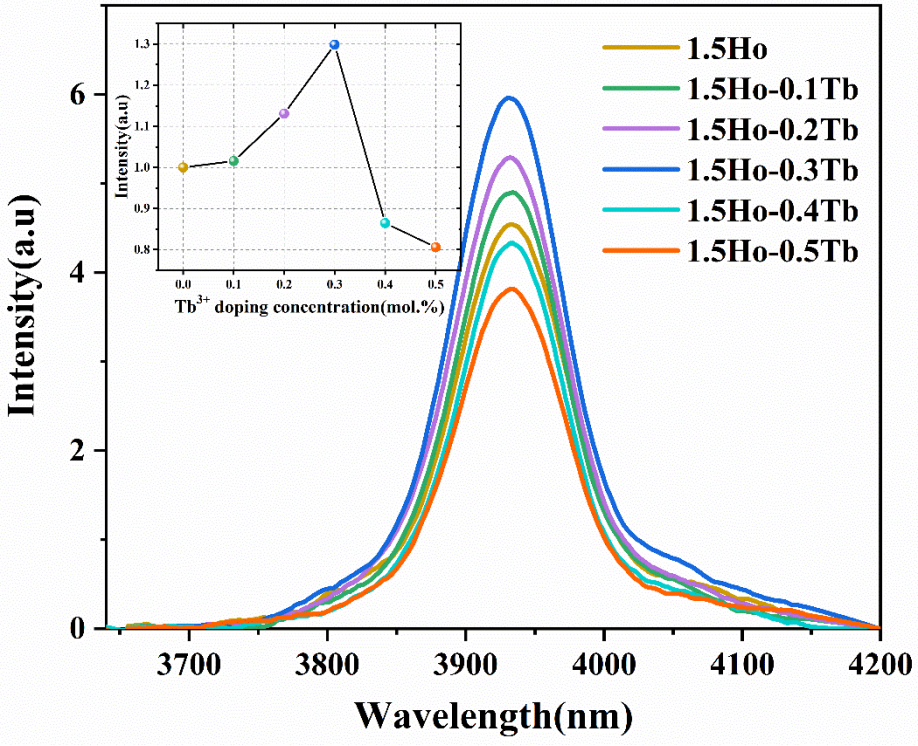

Fig. 3. Emission spectra of Ho^{3+} single-doped and Ho^{3+}/Tb^{3+} co-doped glasses in the wavelength region 3650-4200 nm. Inset: dependence of the luminescence intensity on the concentration of Tb^{3+} ions.

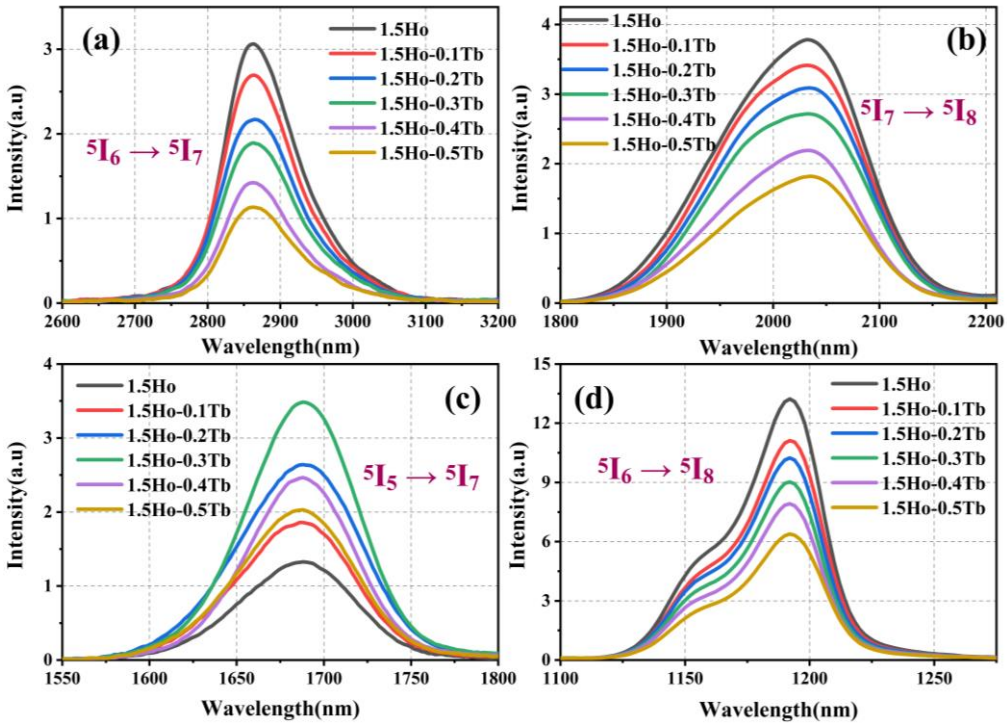

Fig. 4. Fluorescence spectra of Ho^{3+} single-doped and Ho^{3+}/Tb^{3+} co-doped fluoroindate glasses in the wavelength region (a)2600-3200 nm; (b)1800-2200 nm; (c) 1550-1800 nm; and (d)1100-1280 nm.

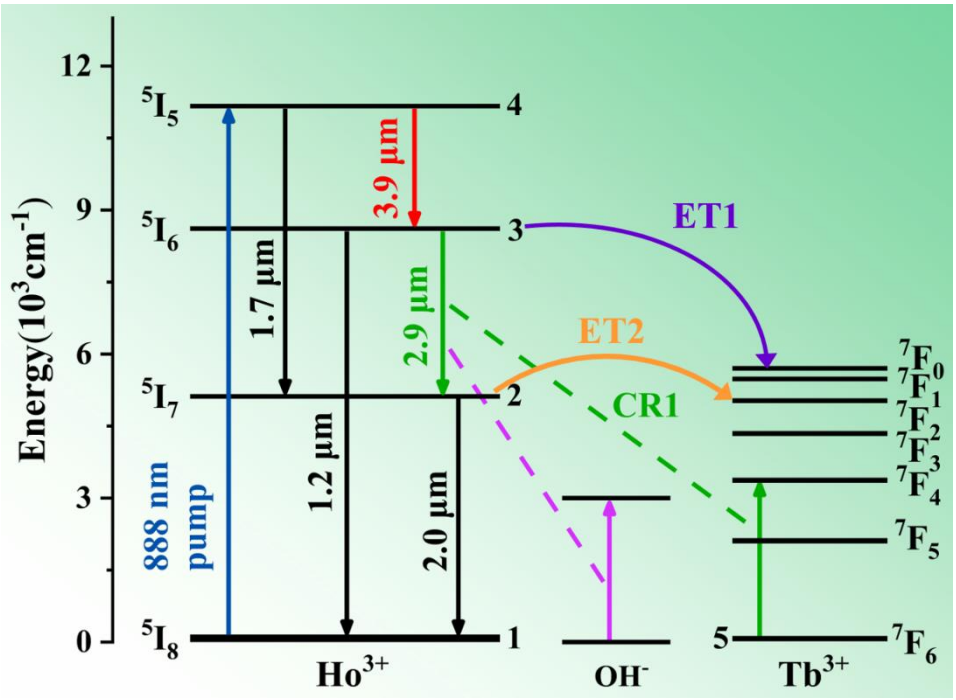

Fig. 5. Energy level diagram and energy transfer process between Ho^{3+} and Tb^{3+} under 888 nm LD excitation.

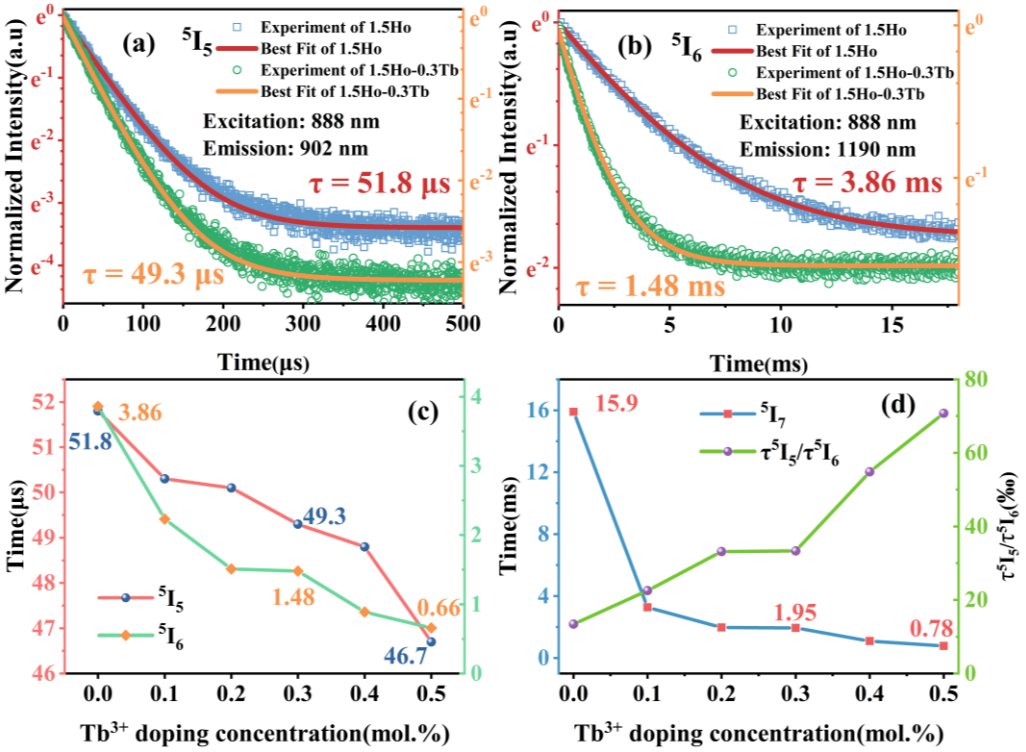

Fig. 6. Luminescence decay curves of (a) the $^5I_5$ and (b) the $^5I_6$ energy levels; (c) experimental lifetimes of $^5I_5$ and $^5I_6$ levels; (d) measured lifetime of the $^5I_7$ level and the dependence of the $^5I_5$ to $^5I_6$ lifetime ratio for different Tb^{3+} concentrations.

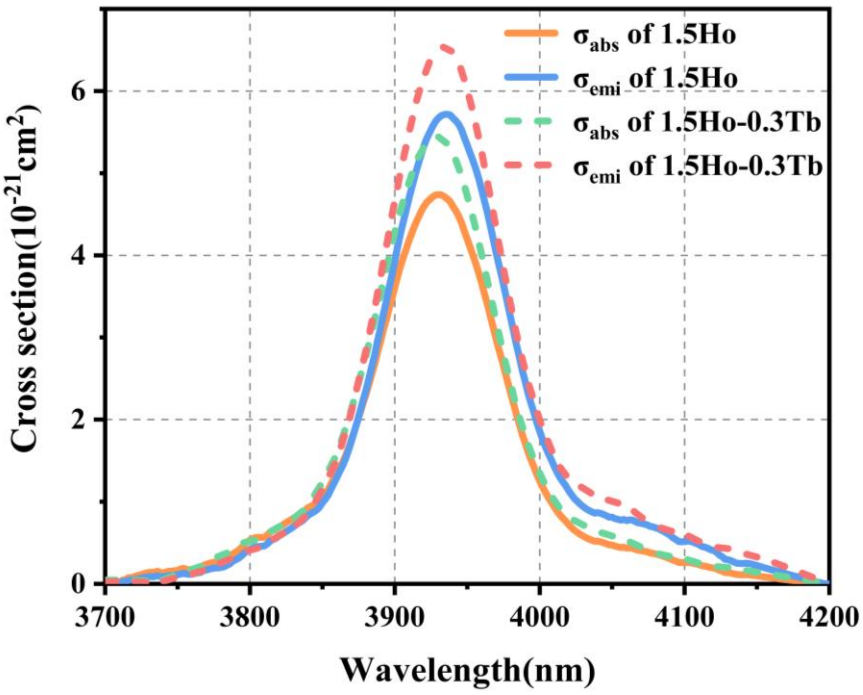

Fig. 7. Absorption and emission cross-sections corresponding to $^5I_5 \rightarrow {}^5I_6$ transitions of Ho^{3+} in single-doped (solid line) and Ho^{3+}/Tb^{3+} co-doped (dash line) fluoroindate glasses.

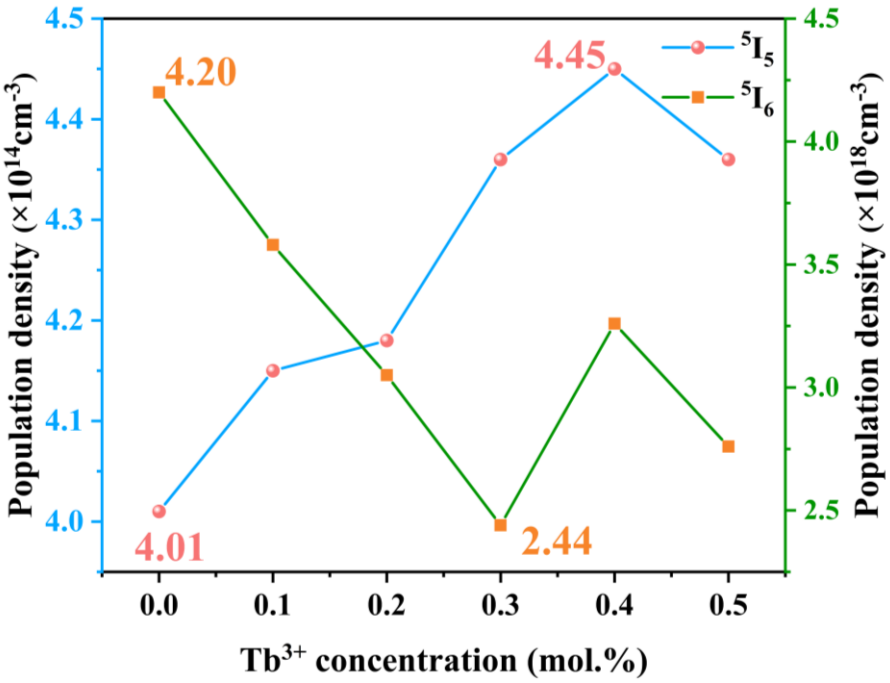

Fig. 8. Population densities of $^5I_5$ and $^5I_6$ levels in glasses with different Tb^{3+} concentration.